Available online at www.sciencedirect.com
ScienceDirect
International Journal of Heat and Mass Transfer 51 (2008) 1596–1602
International Journal of HEAT and MASS TRANSFER
www.elsevier.com/locate/ijhmt

Entropy generation of vapor condensation in the presence of a non-condensable gas in a shell and tube condenser

Y. Haseli, I. Dincer *, G.F. Naterer

Faculty of Engineering and Applied Science, University of Ontario Institute of Technology, 2000 Simcoe Street North, Oshawa, Ontario, Canada L1H 7K4

Received 13 March 2007
Available online 14 September 2007

Abstract

This article investigates the entropy production of condensation of a vapor in the presence of a non-condensable gas in a counter-current baffled shell and one-pass tube condenser. The non-dimensional entropy number is derived with respect to heat exchange between the bulk fluid and condensate, as well as heat exchange between the condensate and coolant. Numerical results show that heat transfer from the condensate to the coolant has a dominant role in generating entropy. For example, at an air mass flow rate of 330 kg/h, 93.4% of the total entropy generation is due to this source. The resultant profiles during the condensation process indicate that a higher air mass flow rate leads to a lower rate of entropy production. For example, as the air mass flow rate increases from 330 kg/h to 660 kg/h and 990 kg/h, the total entropy generation decreases from 976 J/s K to 904 and 857.2 J/s K, respectively. By introducing a new parameter called the condensation effectiveness, a correlation is also developed for predictions of the entropy number, and an illustrative example is presented.

Keywords: Entropy generation; Condensation; Shell and tube condenser; Heat transfer

1. Introduction

Past studies have shown two main sources of irreversibilities in heat exchangers: (i) friction irreversibility due to a pressure drop of fluid streams and (ii) thermal irreversibility due to heat exchange across finite temperature differences. Often the temperature difference has a dominant influence on the value of the overall entropy production [1]. Lin et al. [2] conducted a second-law analysis for a saturated FC-22 vapor flowing through horizontal cooling tubes in a condenser. They reported an optimal cooling temperature that generates a minimum of entropy for a given duty parameter, which depends strongly upon many process parameters, e.g. mass flow rate and tube geometry. Ogulata et al. [3,4] studied a manufactured plate-type cross-flow heat exchanger through the minimum entropy generation number with respect to the second law of thermodynamics. They [4] stated that the minimum entropy generation number depends on parameters such as optimum flow path length, dimensionless mass velocity, dimensionless heat transfer area and dimensionless heat transfer volume. Galovic et al. [5] have presented analytical solutions for the temperature variation of two streams in parallel flow, counter flow and cross-flow heat exchangers, leading to entropy generation due to heat exchange between the streams. In their study, relative entropy generation is defined as the ratio of actual entropy to its maximum value and it is related to the exchanger effectiveness.

Li and Yang [6] performed a thermodynamic analysis of a saturated vapor flowing slowly onto and condensing on an elliptical cylinder. The authors showed how a geometrical parameter, ellipticity, affects entropy generation during a film-wise condensation process. They also obtained an expression for the minimum entropy generation in laminar film condensation. Johannessen et al. [7] have shown that the entropy production due to thermal irreversibility in a

* Corresponding author. Tel.: +1 905 721 3111; fax: +1 905 721 3140.
E-mail addresses: yousef.haseli@mycampus.uoit.ca (Y. Haseli), ibrahim.dincer@uoit.ca (I. Dincer), greg.naterer@uoit.ca (G.F. Naterer).

0017-9310/$ - see front matter © 2007 Elsevier Ltd. All rights reserved.
doi:10.1016/j.ijheatmasstransfer.2007.07.032

Nomenclature

c_p	specific heat, J/kg K
D	diffusion coefficient, m^2/s
d	outer tube diameter, m
h	heat transfer coefficient, W/m^2 K
h_{ol}	heat transfer coefficient from the interface to the cooling water, W/m^2 K
$\dot{m}$	mass flow rate, kg/s
N	entropy generation number
N_t	condensation rate per unit area, kg/m^2s
q	heat flux per unit area, W/m^2
Re	Reynolds number
$\dot{S}$	entropy generation rate (kW/K)
Sc	Schmidt number
T	temperature, °C
W_i	air mass fraction at interface
W_b	air mass fraction at bulk
y	mole fraction

Greek symbols

ε	Ackerman modification factor, Eq. (2)
λ	condensation latent heat, kJ/kg
ρ	density, kg/m^3
ψ	condensation effectiveness

Subscripts

c	coolant
g	vapor–non-condensable mixture
i	interface
v	vapor

heat exchanger is a minimum when the local entropy production is constant throughout all parts of the system. The solution for the minimum was shown to be independent of the heat transfer coefficient.

A new design strategy, involving losses due to fluid and heat transfer irreversibilities that lead to production of entropy, has been recently presented by Lerou et al. [8] and applied to the thermal design of a counter-flow heat exchanger. Adeyinka and Naterer [9] investigated the physical significance of entropy production and a resulting optimization correlation for laminar film condensation on a flat plate. In another entropy analysis of Galovic [10] in evaporator/condenser types of heat exchangers, a model was developed to calculate the overall entropy generation of heat exchange for given values of heat transfer effectiveness and ratios of flow rates.

In contrast to these past studies, this article focuses on the effects of non-condensable gases on heat and mass transfer rates, specifically how they contribute to irreversibilities and entropy production. In this paper, the entropy generation rate is formulated for condensation of a pure vapor in the presence of a non-condensable gas, within a horizontal counter-current baffled E-type shell with a one-path tube condenser. The thermal irreversibility of heat exchange between the bulk fluid and condensate, as well as heat exchange between the condensate and coolant, are taken into account. The relevant entropy generation numbers are established and shown as functions of the non-dimensional temperature and heat transfer coefficient.

2. Thermodynamic analysis

Fig. 1 shows schematically the local conditions at a point on the cooling surface of a steadily operating condenser. A coolant at a temperature of T_c is flowing along the left side of the tube wall. The non-condensable component of the mixture, containing a mean mole fraction of y_v

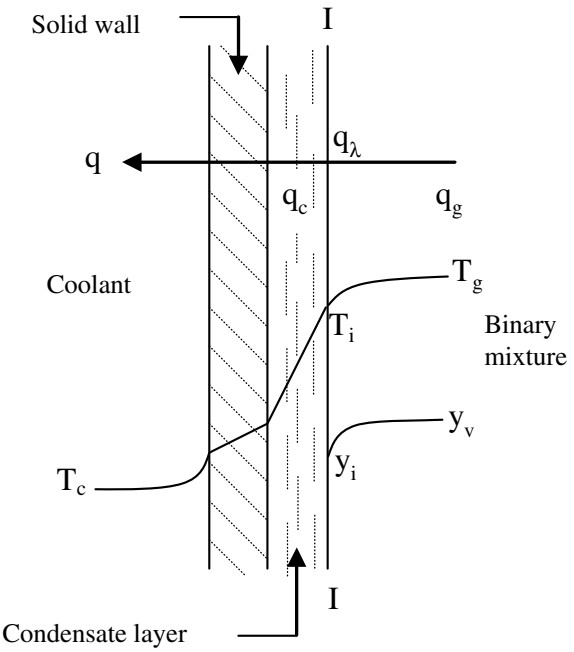

Fig. 1. Schematic of condensation process.

flows at a temperature of T_g past the right face of the wall, and it is separated from that face by a film of condensate. The local heat flux per unit area, q, absorbed by the coolant is the sum of three quantities: q_g, the sensible heat received from the mixture bulk; q_c, the sensible heat of cooling the condensate; and q_λ, the latent heat released by condensation at interface I–I. Usually q_g and q_c are small compared to q_λ [11].

An energy balance for the system gives

$$h_{ol}(T_i - T_c) = h_g \varepsilon (T_g - T_i) + N_t \lambda \quad (1)$$

In this equation, ε is the Ackerman modification factor and h_{ol} is the heat transfer coefficient from the interface to the coolant, where

$$\varepsilon = \frac{N_t c_{pg}/h_g}{1-\exp(-N_t c_{pg}/h_g)} \tag{2}$$

$$\frac{1}{h_{ol}} = \frac{1}{h_{cond.}} + \frac{1}{h_{tw}} + \frac{1}{h_c} + \text{Other resistances} \tag{3}$$

The first term on the right side of Eq. (1) represents the sensible heat transferred from the bulk fluid to the condensate layer, whereas the second term represents the latent heat term. The left side of the equation reflects the total heat absorbed by the coolant.

For a fixed control volume with an effective heat and mass transfer area of A_{cv} shown in Fig. 2, it is assumed that the inlet temperatures of the mixture and coolant are known and the interface temperature is constant. The entropy generation rate due to thermal irreversibilities can be determined as follows:

$$d\dot{S} = dq_{sensible}\left(\frac{T_g - T_i}{T_g T_i}\right) + dq_{tot}\left(\frac{T_i - T_c}{T_i T_c}\right) \tag{4}$$

$$d\dot{S}_1 = dq_{sensible}\left(\frac{T_g - T_i}{T_g T_i}\right) \tag{5}$$

$$d\dot{S}_2 = dq_{tot}\left(\frac{T_i - T_c}{T_i T_c}\right) \tag{6}$$

The heat transfer equation, Eq. (1), over a differential heat transfer area can be alternatively written as

$$\delta q = h_{ol}(T_i - T_c)dA = (h_g \varepsilon (T_g - T_i) + N_t \lambda)dA$$
$$0 \leqslant A \leqslant A_{cv} \tag{7}$$

Hence

$$\dot{S}_1 = \int_0^{A_{cv}} h_g \varepsilon (T_g - T_i)\left(\frac{T_g - T_i}{T_g T_i}\right)dA \Rightarrow$$

$$\dot{S}_1 = \int_0^{A_{cv}} h_g \varepsilon \frac{(T_g - T_i)^2}{T_g T_i}dA \tag{8}$$

The energy conservation equation for the mixture side is

$$\dot{m}_g c_{pg} dT_g = -h_g b (T_g - T_i)dA, \tag{9}$$

where

$$b = \frac{N_t c_{pv}/h_g}{\exp(N_t c_{pv}/h_g) - 1} = \varepsilon \cdot \exp(-N_t c_{pv}/h_g) \tag{10}$$

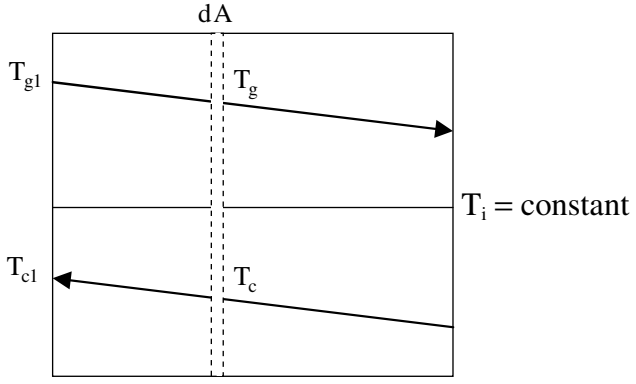

Fig. 2. Control volume with an effective transfer surface of A_{cv}.

Integrating the previous energy equation, subject to a boundary condition of $A = 0$, $T_g = T_{g1}$ yields

$$\frac{T_g - T_i}{T_{g1} - T_i} = \exp\left(-\frac{h_g b A}{\dot{m}_g c_{pg}}\right) \tag{11}$$

Hence, Eq. (8) can be rewritten as

$$\dot{S}_1 = h_g \varepsilon \int_0^{A_{cv}} \frac{(T_{g1} - T_i)^2 \exp\left(-\frac{2h_g b A}{\dot{m}_g c_{pg}}\right)}{T_i\left[T_i + (T_{g1} - T_i)\exp\left(-\frac{h_g b A}{\dot{m}_g c_{pg}}\right)\right]}dA$$
$$= h_g \varepsilon \left(\frac{T_{g1} - T_i}{T_i}\right)^2 \int_0^{A_{cv}} \frac{\exp\left(-\frac{2h_g b A}{\dot{m}_g c_{pg}}\right)}{1 + \left(\frac{T_{g1}}{T_i} - 1\right)\exp\left(-\frac{h_g b A}{\dot{m}_g c_{pg}}\right)}dA \tag{12}$$

Introducing the following non-dimensional parameters,

$$T_g^* = \frac{T_{g1}}{T_i}, \quad h_g^* = \frac{h_g b A_{cv}}{\dot{m}_g c_{pg}}, \quad A^* = \frac{A}{A_{cv}} \tag{13}$$

which allows us to write Eq. (12) in the following form,

$$\dot{S}_1 = h_g \varepsilon A_{cv}\left(T_g^* - 1\right)^2 \int_0^1 \frac{\exp\left(-2h_g^* A^*\right)}{1 + \left(T_g^* - 1\right)\exp\left(-h_g^* A^*\right)}dA^* \tag{14}$$

The solution for integration in Eq. (11) becomes

$$\dot{S}_1 = \frac{h_g \varepsilon A_{cv}}{h_g^*}\left\{\ln\left[\frac{1 + \left(T_g^* - 1\right)\exp\left(-h_g^*\right)}{T_g^*}\right] + \left[\left(T_g^* - 1\right)\left(1 - \exp\left(-h_g^*\right)\right)\right]\right\} \tag{15}$$

In order to determine the entropy generation rate due to heat transfer from the interface to the coolant, Eqs. (6) and (7) are combined as follows:

$$\dot{S}_2 = \int_0^{A_{cv}} h_{ol}\frac{(T_i - T_c)^2}{T_i T_c}dA \tag{16}$$

The energy conservation equation for the coolant is

$$\dot{m}_c c_{pc} dT_c = -h_{ol}(T_i - T_c)dA \tag{17}$$

Integrating again with $A = 0$, $T_c = T_{c1}$ yields

$$\frac{T_i - T_c}{T_i - T_{c1}} = \exp\left(\frac{h_{ol} A}{\dot{m}_c c_{pc}}\right) \tag{18}$$

Hence

$$\dot{S}_2 = h_{ol}\int_0^{A_{cv}} \frac{(T_i - T_{c1})^2 \exp\left(\frac{2h_{ol}A}{\dot{m}_c c_{pc}}\right)}{T_i\left[T_i - (T_i - T_{c1})\exp\left(\frac{h_{ol}A}{\dot{m}_c c_{pc}}\right)\right]}dA$$
$$= h_{ol} A_{cv}(1 - T_c^*)^2 \int_0^1 \frac{\exp\left(2h_{ol}^* A^*\right)}{1 - \left(1 - T_c^*\right)\exp\left(h_{ol}^* A^*\right)}dA^* \tag{19}$$

where

$$T_c^* = \frac{T_{c1}}{T_i}, \quad h_{ol}^* = \frac{h_{ol}A_{cv}}{\dot{m}_c c_{pc}} \tag{20}$$

Similarly, we may derive the following equation for the entropy generation rate,

$$\dot{S}_2 = \frac{h_{ol}A_{cv}}{h_{ol}^*}\left\{\ln\left[\frac{T_c^*}{1-(1-T_c^*)\exp\left(h_{ol}^*\right)}\right] + \left[\left(1-T_c^*\right)\left(1-\exp\left(h_{ol}^*\right)\right)\right]\right\} \tag{21}$$

The entropy generation numbers can now be obtained after dividing Eqs. (15) and (21) by $\dot{m}_c c_{pc}$ and considering the definition of b, h_g^* and h_{ol}^* in Eqs. (10), (13) and (20), respectively, thereby yielding

$$N_1 = \frac{\dot{S}_1}{\dot{m}c_{pc}} = \exp(C)\cdot C_m\left\{\ln\left[\frac{1+\left(T_g^*-1\right)\exp\left(-h_g^*\right)}{T_g^*}\right] + \left[\left(T_g^*-1\right)\left(1-\exp\left(-h_g^*\right)\right)\right]\right\} \tag{22}$$

$$N_2 = \frac{\dot{S}_2}{\dot{m}c_{pc}} = \ln\left[\frac{T_c^*}{1-(1-T_c^*)\exp\left(h_{ol}^*\right)}\right] + \left[\left(1-T_c^*\right)\left(1-\exp\left(h_{ol}^*\right)\right)\right] \tag{23}$$

where C and C_m are two other non-dimensional parameters defined as

$$C = \frac{N_t c_{pv}}{h_g}, \quad C_m = \frac{\dot{m}_g c_{pg}}{\dot{m}_c c_{pc}} \tag{24}$$

In practice, $\left(1+\left(T_g^*-1\right)\exp\left(-h_g^*\right)\right)/T_g^*$ and $T_c^*/(1-\left(1-T_c^*\right)\exp\left(h_{ol}^*\right))$ are nearly close to unity. In this case, Eqs. (22) and (23) can be rearranged as follows:

$$N_1 = \exp(C)\cdot C_m\cdot\left[\left(T_g^*-1\right)^2\left(1-\exp\left(-h_g^*\right)\right)\right]\Big/T_g^* \tag{25}$$

$$N_2 = \frac{\left(1-T_c^*\right)^2\left[\exp\left(h_{ol}^*\right)-1\right]\cdot\exp\left(h_{ol}^*\right)}{1-\left(1-T_c^*\right)\exp\left(h_{ol}^*\right)} \tag{26}$$

It can be observed that in the case of condensation of a saturated pure vapor, i.e., $T_g^* = 1$, entropy production due to sensible heat transfer from the bulk fluid to the interface/condensate layer is zero, so that the total entropy generation will be due to the heat transfer from the interface to the coolant.

3. Results and discussion

Numerical results of the entropy production in a typical horizontal counter-current shell and one-pass tube condenser are presented in this section. Table 1 gives the geometrical features of the condenser and inlet values for a steam–air mixture, with cooling water as the coolant [12]. Each baffle space is defined as a control volume. The calculation algorithm presented by Haseli and Roudaki [12] is used to determine the non-dimensional and other parameters presented in the previous section. Selected results have been verified through comparisons with experiments in Table 2. Table 2 reveals that the calculated performance parameters are in good agreement with the experimental data, thereby providing useful validation of the predictive formulation.

Table 1
Specifications of the condenser

Geometrical specification	
Shell inside diameter (mm)	438.2
Tube outside diameter (mm)	19.05
Tube inside diameter (mm)	14.9
Tube pitch (mm)	25.4
Tube length (mm)	2438
Layout angle (deg)	30
Tube heat conductivity (W/m K)	38
Baffle spacing cut (% of Ds)	35.5
Inlet baffle spacing length (mm)	302
Outlet baffle spacing length (mm)	302
Central baffle spacing length (mm)	300
Total tube number	196
Shell-to-tube bundle clearance (mm)	204
Shell-to-baffle clearance (mm)	5
Baffle-to-tube clearance (mm)	0.4
Inlet conditions of steam–air mixture and cooling water	
Steam–air mixture inlet temperature (°C)	125
Steam inlet mass flow rate (kg/h)	3600
Air mass flow rate (kg/h)	330
Cooling water inlet temperature (°C)	10.5
Cooling water mass flow rate (kg/h)	225,000
Total pressure of condenser (kPa)	18.2

Table 2
Comparison of predicted and measured performance parameters

Quantity	Prediction	Measured
Steam–air mixture outlet temperature (C)	26.7	29.3
Cooling water outlet temperature (C)	20.2	20.05
Outlet steam mass flow rate (kg/h)	27.5	35
Total heat removed to the cooling water (kW)	2570	2500

Source: Ref. [12].

In Fig. 3, the predicted data based on the above approach (from Section 2) is compared with the theory of Rose [13] for forced-convection condensation on a single horizontal tube in the presence of a non-condensing gas. In this case,

$$\frac{qd}{\lambda\rho_g D} = 0.5Re_g^{1/2}\left\{\left[1+2.28Sc^{1/3}\left(\frac{W_i}{W_b}-1\right)\right]^{1/2}-1\right\} \tag{27}$$

where q is the heat flux transferred to the coolant, d is the outer tube diameter, Sc is the Schmidt number, and W_i and W_b represent air mass fractions at the interface and vapor bulk, respectively.

Fig. 3 shows predicted data for condensation from steam–air mixtures on a bank of tubes, plotted as the difference in the air-mass fraction between the bulk vapor

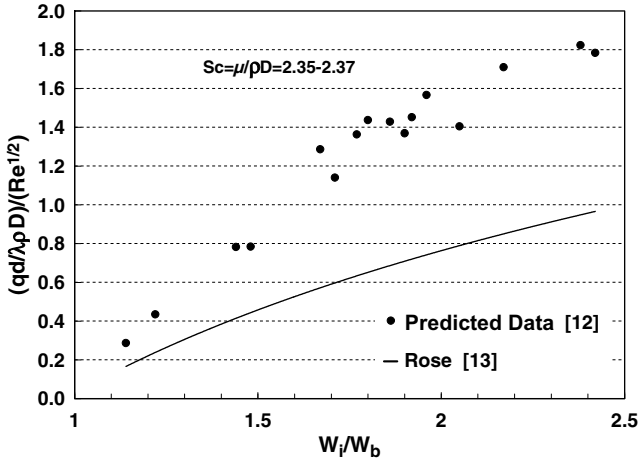

Fig. 3. Comparison of predicted data based on proposed algorithm by Haseli and Roudaki for tube bundle with single tube theory of Rose.

and the condensate surface. The results are compared with the theoretical model of Rose [13]. It can be seen that the data for the tube bank are higher than results of the single tube theory of Rose. This trend was also observed in the experiments of Briggs and Sabaratnam [14,15] where the single tube theory of Rose under-predicted their data related to condensation of steam–air mixture on a bank of tubes. Fig. 3 appears as a kind of general confirmation of the model. As seen in this figure, the single tube theory of Rose under-predicts the performance. Increased mixing and re-circulation of the steam–air mixture down the tube bank may be acting to enhance the heat transfer, compared to the situation of a single tube.

In Fig. 4, the entropy generation rates along the condenser are illustrated. The entropy production due to both sources is significantly higher in the first baffle space, than the last ones. The condensation rate is higher in the first few baffle spaces, and the consequent entropy generation is larger in the first half of the condenser. In addition, as the superheated steam enters the condenser, there is a considerable difference between the bulk and condensate temperatures at the entrance baffle spaces. As condensation occurs along the condenser, the temperature difference and mass flow rate of the mixture are reduced. Thus, entropy generation due to sensible heat exchange decreases.

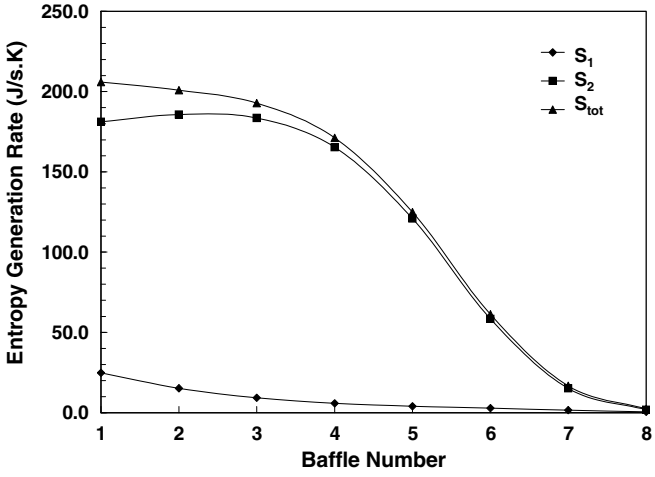

Fig. 4. Calculated entropy generation rate along the condenser.

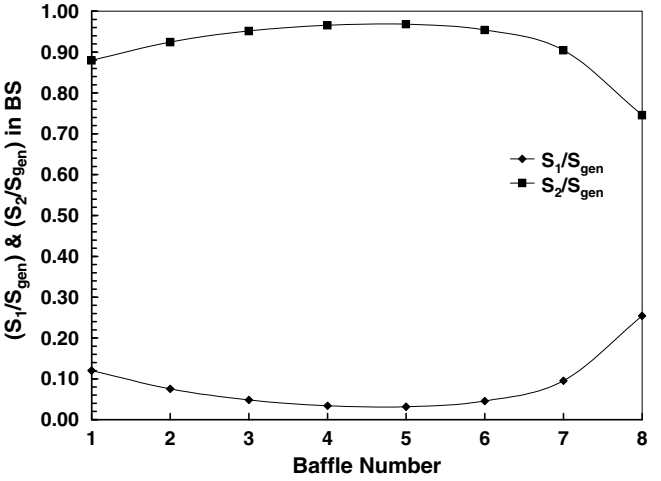

Fig. 5. Ratio of entropy generation rates to total entropy generation rate in each baffle space.

The ratio of the entropy generation rate, due to each source of total entropy generation in each baffle space, is shown in Fig. 5. Approximately 90% of entropy generation is due to the total heat absorbed by the cooling water. The sudden increase (decrease) of the lower (upper) curve at the end of the heat exchanger (air cooled part of the condenser) is due to the considerable decrease of the steam condensation rate and reduced bulk side temperature.

Fig. 6 illustrates the variation of entropy generation numbers along the condensation path for three different air leakages, which allows us to observe the effect of the presence of air as non-condensable gas on entropy production. As air leakage increases, heat and mass transfer decreases which, consequently, reduces the entropy generation. According to Fig. 6, between the fifth and sixth baffle spaces, entropy profiles contact each other. After this

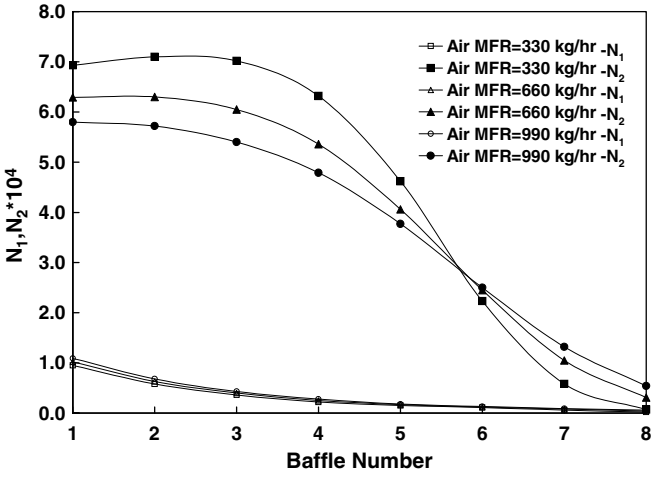

Fig. 6. Variation of entropy generation number along the condensation path for different air.

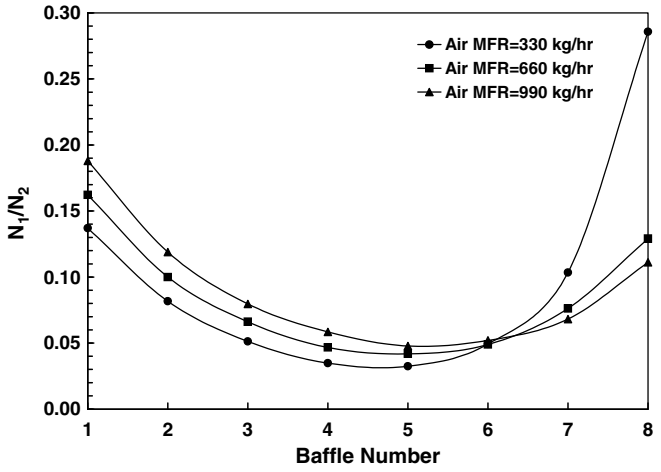

Fig. 7. Ratio of entropy number due to sensible heat exchange to the entropy number due to heat transfer to the cooling water.

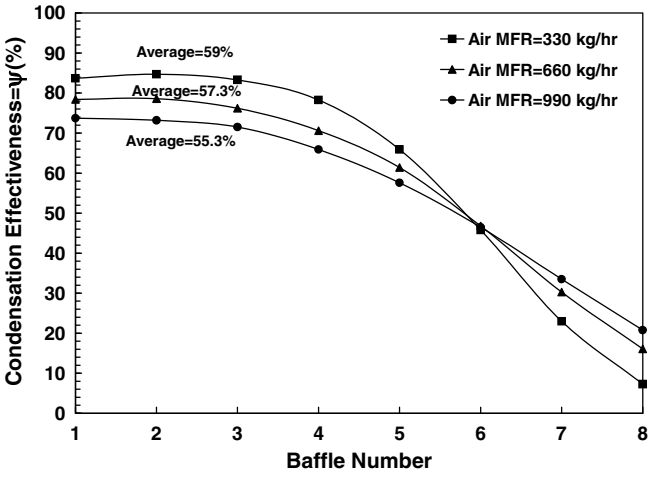

Fig. 8. Condensation effectiveness, ψ, along the condenser for three different air leakages.

region, because of the larger steam fraction at the larger air mass flow rate, condensation occurs faster and therefore the corresponding profile is higher.

The variation of the ratio of two entropy generation rates is shown in Fig. 7. It can be observed that each curve has a minimum, which moves up and the related curve becomes wider as the air flow increases. As mentioned previously, air is a non-condensable gas that resists the heat and mass transfer. Increasing the air leakage causes a decrease in the condensation heat transfer rate, so the role of sensible heat exchange will increase in the process. This suggests that the corresponding entropy generation numbers will be affected in the same way. It should be noted that for condensation of a saturated vapor, we would expect an exponential trend for the curves in Fig. 6. In this case, the first part from the steam–air entrance to the sixth baffle space, where all profiles cross each other, is approximately flat as there is no significant temperature drop in the bulk side.

Define the following parameter called the condensation effectiveness, which represents the ratio of the condensation rate to the maximum possible condensation rate:

$$\psi = \frac{N_t}{N_{t,\max}} \tag{28}$$

where $N_{t,\max}$ refers to the condensation of saturated pure vapor (without the presence of a non-condensable gas). It is required to re-calculate the condensation temperature, T_i, while the same values of the temperature at the inlet of the baffle space will be used to determine the maximum condensation rate in each baffle space. The resulting profiles for condensation effectiveness at different air mass flow rates are shown in Fig. 8. As expected, increasing the air leakage leads to a lower condensation effectiveness. For air mass flow rates of 330 kg/h, 660 kg/h and 990 kg/h, the average condensation effectivenesses are 59%, 57.3% and 55.3%, respectively. The variation of the entropy number, N_2, with condensation effectiveness is shown in Fig. 9. At a higher

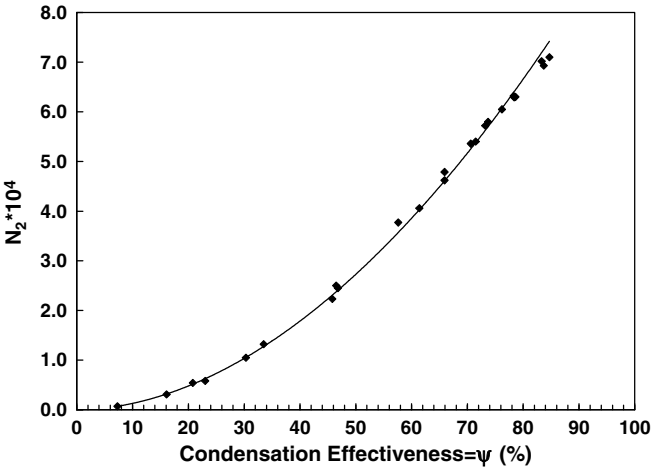

Fig. 9. Dependence of entropy number on condensation effectiveness.

effectiveness, condensation heat transfer is higher and it results in larger entropy generation. It can be observed that the relation between N_2 and ψ is similar to a power-type function. We propose the following correlation which predicts the entropy number with less than 0.1% error:

$$N_2 = 10.175 \times 10^{-4}\psi^{1.8994} \quad 0 \leqslant \psi \leqslant 1 \tag{29}$$

This provides a useful design correlation for improving performance of the heat exchangers.

4. Conclusions

The non-dimensional entropy generation number for condensation of a pure vapor in the presence of a non-condensable gas is derived for a counter-current shell and one-pass tube condenser. It is shown that the entropy number related to sensible heat exchange is a function of the non-dimensional heat capacity, temperature and heat transfer coefficient, whereas the function due to total heat received by the coolant depends on two factors: non-dimensional

temperature and heat transfer coefficient. In the case of condensation of a saturated pure vapor, the entropy generation caused by sensible heat exchange will vanish. The dominant source of entropy production is due to the total heat exchange between condensate and coolant. The resulting entropy profiles are determined form a numerical solution algorithm, which shows that increasing the air mass flow rate causes a decrease of the entropy production. Additionally, a correlation is presented for the entropy number, in terms of a new parameter called the condensation effectiveness.

Acknowledgement

The authors acknowledge the support provided by the Natural Sciences and Engineering Research Council of Canada in Canada.

References

[1] A. Bejan, Advanced Engineering Thermodynamics, John Willey & Sons, New York, 1988.
[2] W.W. Lin, D.J. Lee, X.F. Peng, Condensation performance in horizontal tubes with second law consideration, Int. J. Energy Res. 25 (2001) 1005–1018.
[3] R.T. Ogulata, F. Duba, T. Yilmaz, Irreversibility analysis of a cross flow heat exchangers, Energy Conserv Manage 41 (2000) 1585–1599.
[4] R.T. Ogulata, F. Duba, T. Yilmaz, Second law and experimental analysis of a cross flow heat exchanger, Heat Transfer Eng. 20 (1999) 20–27.
[5] A. Galovic, Z. Virag, M. Zivic, Analytical entropy analysis of recuperative heat exchangers, Entropy 5 (2003) 482–495.
[6] G.C. Li, S.A. Yang, Entropy generation minimization of free convection film condensation on an elliptical cylinder, Int. J. Therm. Sci. 47 (2007) 407–412.
[7] E. Johannessen, L. Nummedal, S. Kjelstrup, Minimizing the entropy production in heat exchange, Int. J. Heat Mass Transfer 45 (2002) 2649–2654.
[8] P.P.P.M. Lerou, T.T. Veenstra, J.F. Burger, H.J.M. ter Brake, H. Rogalla, Optimization of counter flow heat exchanger geometry through minimization of entropy generation, Cryogenics 45 (2005) 659–669.
[9] O.B. Adeyinka, G.F. Naterer, Optimization correlation for entropy production and energy availability in film condensation, Int. Commun. Heat Mass Transfer 31 (2004) 513–534.
[10] A. Galovic, Non-dimensional entropy analysis of evaporator and/or condenser type heat exchangers, Int. J. Heat Exchang. V (2004) 1524–5608.
[11] A.P. Colburn, T.B. Drew, The condensation of mixed vapors, Trans. Am. Inst. Chem. Eng. 33 (1937) 197–215.
[12] Y. Haseli, S.J.M. Roudaki, A calculation method for analysis condensation of a pure vapor in the presence of a non-condensable gas on a shell and tube condenser, Proceedings of the ASME Heat Transfer/Fluids Engineering Conf., Charlotte, NC, 2004; vol. 3, pp. 155–163.
[13] J.W. Rose, Approximate equations for forced-convection condensation in the presence of a non-condensing gas on a flat plate and horizontal tube, Int. J. Heat Mass Transfer 23 (1980) 539–546.
[14] A. Briggs, S. Sabaratnam, Condensation of steam in the presence of air on a single tube and a tube bank, Int. J. Energy Res. 27 (2003) 301–314.
[15] A. Briggs, S. Sabaratnam, Condensation from pure steam and steam–air mixtures on integral-fin tubes on a bank, ASME J. Heat Transfer 127 (2005) 571–580.